Cylindrical Phase of Block Copolymers in Thin Films

Marianne Heckmann* and Barbara Drossel

Institut für Festkörperphysik, Technische Universität Darmstadt, Darmstadt, Germany

Received January 23, 2008; Revised Manuscript Received July 25, 2008

ABSTRACT: We investigate the microphases of diblock copolymers confined in a thin film with walls interacting with the polymer chains. We focus on the possible structures of copolymers that form cylindrical phases in the bulk. By employing self-consistent field theory, we obtain the concentration profile minimizing the free energy of the system. We present a phase diagram showing the possible microphases for a diblock copolymer with fixed volume fraction $f = 0.35$ and fixed segregation parameter $\chi N = 16$ in dependence of the film thickness and the affinity of the walls for the minority monomer. This phase diagram contains only four types of phases, all of which can be understood as a combination of the cylindrical bulk phase and an increased covering of the walls by the preferred monomer type. Other phases, in particular perforated lamellae or several layers of conventional lamellae, are found to be unstable in the investigated parameter regime, when the accuracy of the algorithm is chosen high enough. We perform a careful analysis of the effects of numerical accuracy and compare our work to previous studies that reported perforated lamellae to be a stable phase.

1. Introduction

The ability to control self-assembly in macromolecular systems provides a convenient route to creating various ordered structures at the nanoscale. Diblock copolymer melts cannot exhibit macrophase separation of the two monomer species but do self-assemble into a variety of periodic nanostructures when they undergo a phase transition into the ordered phase. It has been recognized that AB diblock copolymers in the bulk form four thermodynamically stable microphases: lamellae, hexagonally arranged cylinders, body-centered cubic lattices of spheres, and the gyroid morphology.[1−7]

When confined in thin films, diblock copolymers also show mixed structures combining different elements of the bulk phases, and several authors also report completely new structures. Thin films of symmetric diblock copolymers are the ones studied most extensively experimentally[8,9] as well as theoretically.[10−12] Symmetric copolymers form lamellae in the bulk, and when confined to a thin film with neutral walls, the lamellae are found to orient perpendicularly to the walls. With a preference of the walls for one monomer species, the microphases alternate between perpendicular and parallel lamellae as the thickness of the film is varied.[30]

More recent studies focused on films of asymmetric diblock copolymers that have a cylindrical bulk phase. In thin films, the cylinders may not only change their orientation in the film when the film thickness is varied but also be replaced by other morphologies in order to maximize the energetically advantageous contacts of one monomer type with the walls. For instance, theoretical studies based on dynamical density functional theory[13,14] and Monte Carlo simulations[15] predict the following types of phases for a block copolymer with volume fraction $f = 0.33$ and $f = 0.25$, respectively, and different affinities of the walls: parallel cylinders, perpendicular cylinders, parallel lamellae, and parallel perforated lamellae. These four morphologies have also been observed experimentally[16,17] in a thin film system. Other studies employ self-consistent field theory[18] and find additional phases for a diblock copolymer with volume fraction $f = 0.3$, such as undulated cylinders and lamellae. Other SCFT studies, which use the parameter values $f = 0.25$, $\chi N = 25$[19] and $f = 0.29$, $\chi N = 18$,[20] focus on the influence of strong electric fields and therefore consider only a narrow range of wall affinities, for which they report only cylindrical phases when the field has zero strength. The SCFT simulations reported in[21] for $f = 0.34$ produced cylindrical phases with or without lamellae at the walls and perforated lamellae.

It is the purpose of this paper to investigate which of the reported phases are truly stable. None of the previous studies focus on the numerical accuracy of the applied algorithms and the consequences for the stability of different morphologies. Structures such as hexagonally perforated lamellae and undulated cylinders cannot be explained in terms of the bulk phase and an increased wetting of the walls by the preferred monomer type. A careful analysis is therefore required in order to decide whether they can indeed be stable structures.

We apply self-consistent field theory (SCFT) to thin films of asymmetric block copolymers that form a cylindrical phase in the bulk. Since many phases are translationally invariant along a direction parallel to the walls, we first calculate the phase diagram of an effectively two-dimensional system. We use intermediate segregation levels and investigate the influences of both the film thickness and the surface interactions on the microstructure of the films. We find the following four types of stable phases: horizontal and perpendicular lamellae, cylinders, and mixed phases with lamellae at the walls and cylinders in the center of the film. Horizontal lamellae occur only for very thin films when the cylindrical phase does not fit into the film at all and where the wall potential enforces an enrichment of one phase at the walls. Very thin films with a weak wall potential show perpendicular lamellae.

We also study three-dimensional systems and focus on those regions of parameter space where phases may occur that cannot be reduced to two dimensions. Where the two-dimensional systems form perpendicular lamellae, three-dimensional systems form perpendicular cylinders. We find that the phases found depend sensitively on the number of collocation points. Because of their limited number, it is often difficult to decide which structure represents the minimum of the free energy. In many cases, the energies of two different morphologies differ only by about 0.5%. We therefore investigated in more detail the influence of numerical inaccuracies and of the implementation of the confining walls on the free energy of different morphologies. We thus found that undulated structures are artifacts of too few collocation points and that they merely represent almost stationary points of the free energy. For some parameter values,

* To whom correspondence should be addressed.

10.1021/ma8001627 CCC: $40.75
Published on Web 09/24/2008

perforated lamellae seem to be a stable morphology. However, other structures are always very close in free energy, and when we take more collocation points, perforated lamellae do not occur anymore. An equivalent behavior is seen in two-dimensional systems, where pure lamellar phases with more than one lamella vanish when we increase the number of collocation points.

The paper is organized as follows: in section 2, we briefly describe the model we use and the underlying self-consistent field theory. In section 3, we present the phases we find for two- and three-dimensional systems and discuss the phase diagrams for films with two identical walls or with one neutral and one attractive wall. In section 4, we summarize and discuss our results.

2. Model

We consider a system of n AB diblock copolymer chains in a volume V. Each chain has the same length N and composition f. We assume that A and B segments have equal statistical segment length a. Each polymer chain is modeled as a continuous Gaussian chain with radius of gyration $R_G = a\sqrt{N/6}$ and is parametrized by a variable s that increases continuously from $s = 0$ to $s = 1$ along its length. The configuration of the αth polymer is described by the function $\mathbf{r}_\alpha(s)$. In these terms, the dimensionless operator for the A and B segment density is expressed as

$$\hat{\phi}_A(\mathbf{r}) = \frac{N}{\rho_0}\sum_{\alpha=1}^{n}\int_0^f \delta(\mathbf{r} - \mathbf{r}_\alpha(s))\,\mathrm{d}s$$

$$\hat{\phi}_B(\mathbf{r}) = \frac{N}{\rho_0}\sum_{\alpha=1}^{n}\int_0^f \delta(\mathbf{r} - \mathbf{r}_\alpha(s))\,\mathrm{d}s$$

It is a good approximation to assume the polymer mixture to be incompressible, $\hat{\phi}_A + \hat{\phi}_B = 1$. In order to obtain scalar quantities for the concentration profile, we insert the identity $1 = \int \mathcal{D}\Phi\delta(\Phi - \hat{\phi})$ into the partition function of the system. The melt is confined between two walls at $z = 0$ and $z = D_\parallel$.

With the above specification of the system, we can now apply the self-consistent field theory.[3] In the spirit of mean-field theory the free energy, F, of the film is

$$\frac{F}{nk_BT} = -\ln\left(\frac{\mathcal{Q}[W_A, W_B]}{V}\right) + \frac{1}{V}\int \mathrm{d}\mathbf{r}(\chi N\Phi_A(1 - \Phi_A) - W_A\Phi_A - W_B(1 - \Phi_A) + H(\mathbf{r})N(\Phi_A(\mathbf{r}) - \Phi_B(\mathbf{r}))$$

where W_A and W_B are the fields acting on A monomers and B monomers, respectively. The logarithmic term represents the free energy of a chain subjected to the mean fields, and $\mathcal{Q}$ is the partition function of a single chain. The integral gives the contribution of the AB segment interactions to the free energy, where χ is the Flory−Huggins parameter which measures the incompatibility between A and B blocks. The integral also includes an interaction energy due to the surface potential

$$H(\mathbf{r}) \equiv 2(\Lambda_1\delta(z) + \Lambda_2\delta(z - D_\parallel))R_G$$

Λ_1 and Λ_2 denoting the interactions between the blocks and the walls. We use reflecting boundary conditions at the walls, as is also done in ref 22. Such boundary conditions lead to the correct statistical weights for polymer configurations confined between two walls, if one neglects the fact that the polymer concentration vanishes at the surface and that the incompressibility constraint can therefore not be applied very close to it. The single chain partition function $\mathcal{Q}$ can be calculated as

$$\mathcal{Q} = \int \mathrm{d}\mathbf{r}\, q(\mathbf{r}, s)\, q^\dagger(\mathbf{r}, s) \quad (1)$$

where the propagators $q(\mathbf{r},s)$ and $q^\dagger(\mathbf{r},s)$ can be obtained by solving two modified diffusion equations

$$\frac{\partial q(\mathbf{r}, s)}{\partial s} = \begin{cases} \frac{1}{6}Na^2\nabla^2 q(\mathbf{r}, s) - w_A(\mathbf{r})\, q(\mathbf{r}, s) & \text{for } s \le f \\ \frac{1}{6}Na^2\nabla^2 q(\mathbf{r}, s) - w_B(\mathbf{r})\, q(\mathbf{r}, s) & \text{for } s > f \end{cases} \quad (2)$$

and

$$\frac{\partial q^\dagger(\mathbf{r}, s)}{\partial s} = \begin{cases} -\frac{1}{6}Na^2\nabla^2 q^\dagger(\mathbf{r}, s) + w_A(\mathbf{r})\, q^\dagger(\mathbf{r}, s) & \text{for } s \le f \\ -\frac{1}{6}Na^2\nabla^2 q^\dagger(\mathbf{r}, s) + w_B(\mathbf{r})\, q^\dagger(\mathbf{r}, s) & \text{for } s > f \end{cases} \quad (3)$$

The initial conditions of the above equations are $q(\mathbf{r}, 0) = 1$ and $q^\dagger(\mathbf{r}, 1) = 1$. The local segment density can then be calculated to be

$$\phi_A(\mathbf{r}) = \frac{V}{\mathcal{Q}}\int_0^f \mathrm{d}s\, q(\mathbf{r}, s)\, q^\dagger(\mathbf{r}, s) \quad (4)$$

The mean fields can be computed from the segment densities

$$\phi_B(\mathbf{r}) = \frac{V}{\mathcal{Q}}\int_f^1 \mathrm{d}s\, q(\mathbf{r}, s)\, q^\dagger(\mathbf{r}, s) \quad (5)$$

by

$$w_A(\mathbf{r}) - w_B(\mathbf{r}) = 2\chi N(\phi_B(\mathbf{r}) - \phi_A(\mathbf{r})) - 2H(\mathbf{r})N \quad (6)$$

These last two equations have to be solved self-consistently, taking into account the incompressibility constraint. This is done by starting from some initial values for the fields and the segment densities and iterating the last five equations until self-consistency is obtained. The main numerical effort hereby goes into the solution of the differential equations for q and $q^\dagger$. We implement the algorithm developed by Fredrickson and coworkers[23] in which a pseudospectral splitting scheme is used preserving spectral accuracy in space and implementing high-order accuracy in the contour variable s.[23,24] The differential equation (2) is solved by stepping forward in s from the initial condition by means of the formula

$$q(\mathbf{r}, s + \Delta s) = \exp\left(-\frac{\Delta s}{2}w(\mathbf{r})\right) \times \exp(\Delta s\nabla^2)\exp\left(-\frac{\Delta s}{2}w(\mathbf{r})\right)q(\mathbf{r}, s) + \mathcal{O}(\Delta s^3) \quad (7)$$

In order to relax toward mean-field configurations of the concentration profiles, we iterate the following scheme:

1. Initialize the fields w_A and w_B. This can be done by taking random numbers or the fields of a structure already computed.
2. Solve the differential equations (2) and (3) for $q(\mathbf{r},a)$ and $q^\dagger(\mathbf{r},a)$.
3. Calculate $\mathcal{Q}$ and the concentrations ϕ_A and ϕ_B using eqs 1, 4, and 5.
4. Update the fields w_A and w_B using (6).
5. Repeat steps 2−5 until a convergence criterion is satisfied.

The delta potential at the confining walls is implemented as a step function over a small interval to avoid numerical instabilities due to the sharp edge of the potential. We perform the algorithm on a lattice with periodic boundary conditions in the unconfined space directions and reflecting boundary conditions at the walls. When we restrict our analysis to two-dimensional systems, we have to minimize the free energy with respect to the period in the unconfined direction. In three

dimensions, this minimization is not necessary for structures that are effectively two-dimensional and translationally invariant in one direction because they can obtain their preferred periodicity by choosing the appropriate orientation within a two-dimensional unit cell with periodic boundary conditions. For other structures the free energy has to be minimized with respect to the period, but the range in which the period has to be varied is smaller than for two-dimensional systems because there is a set of rotations that satisfy the periodic boundary conditions.

3. Results and Discussion

With the above-described algorithm we are able to study two-dimensional systems as well as three-dimensional ones. The advantage of studying two-dimensional systems is that the number of collocation points increases only quadratically instead of cubically with the desired point density. One can therefore perform the SCFT with higher accuracy. The confinement to two dimensions prohibits perpendicularly oriented cylinders and perforated lamellae. It is reasonable to perform the algorithm in three dimensions only where perforated lamellae or perpendicular structures could be energetically favorable. The number of collocation points is essentially limited by computer memory. Thus, we have to restrict our study to thin films. We focus on films with the same surface potentials at both walls. Because of the way we implement the reflecting boundary conditions, we obtain always structures that are symmetric with respect to the plane in the center of the film. When we are not sure that the equilibrium morphology displays this symmetry, we study instead of the simple film a film with twice its width and with an additional (infinitesimally thin) wall in the middle of the film which has on both sides the same affinity as the two confining walls. One half of this film then corresponds to the film of half-width without an enforced symmetry. By assigning to the central wall an affinity different from that of the two external walls, one would be able to implement a system with different affinities at both walls. For the special case that one wall has no preference for either monomer type, the central wall can be omitted, and we have again the original situation with an enforced symmetry with respect to the central plane.

3.1. Results for Two-Dimensional Systems. We first study a two-dimensional system, assuming the structure to be translationally invariant in the third direction. This rules out structures that are not translationally invariant, such as perforated lamellae- or perpendicular cylinders. Two-dimensional systems could be realized experimentally by confining the polymers to some surface or interface.

The AB diblock copolymer film is specified by the parameters f, $D_{||}$, χN, $\Lambda_1 N$, and $\Lambda_2 N$. We fix two of the control parameters by setting $f = 0.35$ and $\chi N = 16$, so that the block copolymers form hexagonally ordered cylinders in the bulk phase. We assume that the two walls are identical, so that $\Lambda_1 = \Lambda_2 = \Lambda$. $\Lambda > 0$ means a preference of the walls for the A monomers, which we choose to be the minority monomer. Our system describes at the same time a film confined between an attractive and a neutral wall, if we consider only the part between one wall and the center. We vary the distance between the confining walls $3R_G < D_{||} < 13R_G$ and the affinity Λ.

We choose up to 256^2 collocation points to obtain smooth profiles of the microstructures and to get an expression for the free energy with an accuracy of 0.1%. In order to describe the polymer chain with sufficient accuracy, we choose the number of segments in the chain in the same order of magnitude as the number of collocation points. It turns out that the inaccuracy due to the discretization of the chain is smaller than that of the numerical quadrature when we take 300−500 segments for each chain. The error in the partition functions q and $q^\dagger$ is of order $\mathcal{O}(\Delta s^3)$; thus, the inaccuracy in the free energy also scales with Δs^3. We have to be very careful when identifying stable morphologies because their free energies differ in many cases only by about 1−5%. Taking too few collocation points often leads to structures that turn out to be only a local minimum of the free energy when more collocation points are used.

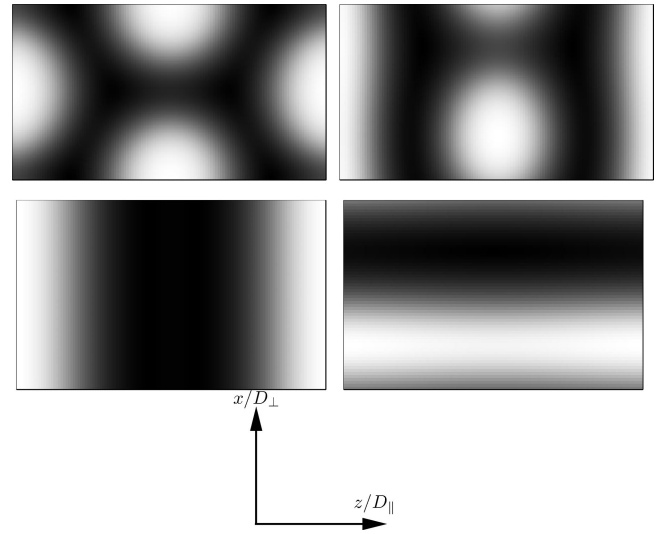

Figure 1. Thermodynamically stable morphologies for a two-dimensional system of an asymmetric diblock copolymer ($f = 0.35$) in a thin film (dark regions represent a high density of B monomers): pure cylindrical phase, mixed cylindrical phase, and pure lamellar phase (oriented parallel and perpendicularly to the surface). The two walls are at the right and left end of each picture, and the pattern is periodically repeated in the vertical direction, which is the direction parallel to the walls.

Because of the affinity of the walls for one of the components of the block copolymer, this component has an increased concentration near the walls. Therefore, there exist more complicated structures than those appearing in the bulk. We can classify these morphologies into four different types (see Figure 1):

- Two types of pure lamellar phases: they form when the film is too thin for cylinders to fit in. When the surface interaction energy between the polymers and walls is weak, the lamellae are perpendicular to the walls; for stronger surface interaction, horizontal lamellae are formed.
- Pure cylindrical phases: they emerge when the wall's affinity for the A monomers is not too high and when the film thickness does not deviate too much from a value preferred by the cylinders.
- Mixed structures with lamellae at the walls and cylinders in the center of the film: when the wall affinity causes a sufficiently large enrichment of the A segments at the walls, lamellae are formed at the walls while cylinders are formed in the center. The transition between the pure cylindrical and the mixed phase occurs at a smaller value of the affinity when the film thickness deviates more from the values preferred by the cylinders.

In Figure 3, we present two phase diagrams showing the different morphologies as a function of the film thickness and the affinity of the walls. The top phase diagram is for a system with an enforced symmetry with respect to the central plane. It is most properly interpreted as the phase diagram of a system of half the width and with one attractive and one neutral wall. The bottom phase diagram is for a system with two identical walls and no imposed symmetry with respect to the central plane. It was obtained by using a film with twice the width and with an additional wall in the middle of the film, which has the same affinity as the two confining walls.

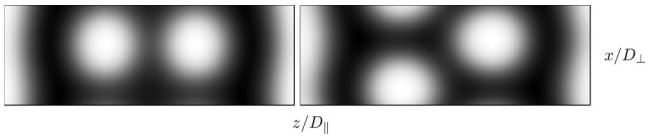

Figure 2. Phases with two rows of cylinders in the center and lamellae at the walls. The pattern is repeated periodically in the vertical direction, which is parallel to the walls. Left: system with an enforced symmetry with respect to the central plane. The two rows of cylinders form a rectangular pattern. Right: half of a system with twice the width and an additional wall in the middle of the film, which is also the symmetry plane. Now the cylinders can arrange hexagonally. The parameters are $\Lambda N = 0.4$ and $D_\parallel = 9R_G$.

The vertical axis of the diagrams denotes the affinity while the horizontal axis denotes the thickness of the film in units of the radius of gyration R_G. For film thickness $D_\parallel < 3R_G$, we always find perpendicularly oriented lamellae, with the A layer becoming thicker close to the walls. We cannot see perpendicularly oriented cylinders because we chose a two-dimensional system. We restrict our analysis to films with $D_\parallel < 13R_G$ because of the computational cost for thicker films, which require more collocation points to obtain reliable results. Knowing that the walls only affect the morphology at a small distance from them, we expect to find the cylindrical bulk morphology in the center of thicker films and wetting lamellae or deformed cylinders at the walls depending on the strength of the interaction. Because of the imposed symmetry, structures with an even number of rows of cylinders are not arranged hexagonally in the top phase diagram, but instead the central two rows form rectangles (see Figure 2).

The two phase diagrams differ only where there is an even number of cylindrical rows in the system, since their arrangement and therefore their energy are different, and in a small region where pure and mixed cylindrical phases are very similar in their free energies.

Near the boundaries between different morphologies the free energies of the adjacent structures only differ by about 0.5−1% or even less. Therefore, both morphologies appear to be stable. We found that the free energy of one structure can change by about 0.5% when comparing the results obtained with 128 and 256 points in the two spatial directions. This is why one has to be very careful when identifying the stable morphologies. In order to be sure to obtain the stable morphology within the errors made due to the number of collocation points, we computed the free energies of the possible structures by first creating the two competing morphologies by choosing two appropriate sets of parameter values and by slowly varying the parameters of the system after the simulations have converged to one of the structures.

Furthermore, the parameter regions where our implementation of the SCFT leads to two different morphologies depending on the initialization become smaller when the number of collocation points increases. Some obtained structures even vanish completely when more collocation points are used. In particular, phases with more than the smallest possible number of horizontal lamellae do not occur any more when the number of collocation points is 256, while they occur very often with 32 collocation points and often have the lowest free energy, even when the correct morphology is a pure cylindrical one.

In order to quantify the influence of the number of collocation points on the accuracy of the free energy, we carefully computed the free energy of a cylindrical phase in dependence of the structure's period $D_\perp$. These results are shown in Figure 4. We see that both the optimal period and the total free energy depend on the number of collocation points.

3.2. Results for Three-Dimensional Systems. In order to identify parameter regions where perforated lamellae and perpendicularly oriented cylinders might occur, we next performed the calculations in three dimensions.

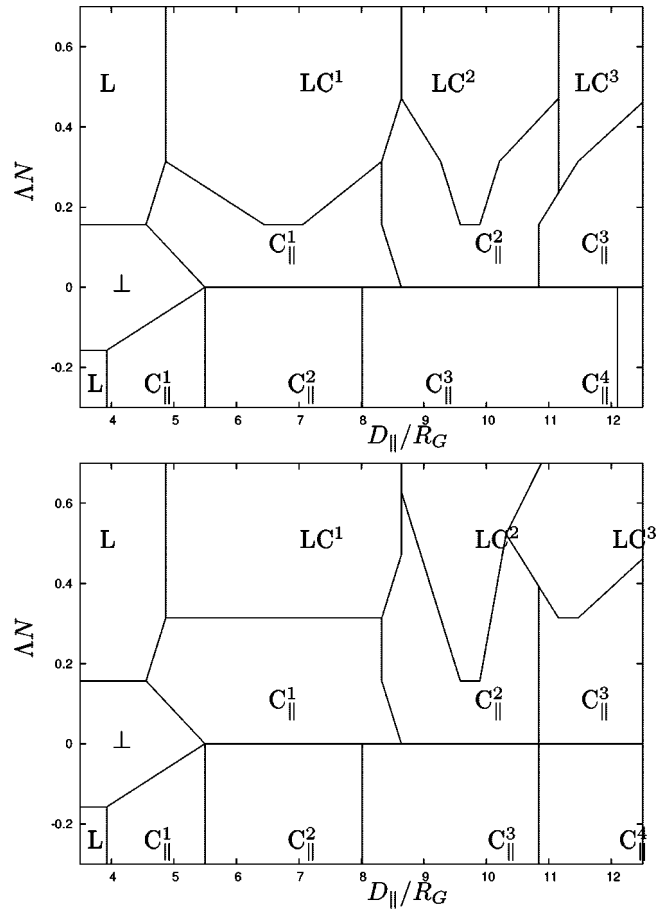

Figure 3. Phase diagram for a diblock copolymer with $f = 0.35$ and $\chi N = 16$ in a thin film with two identical walls with (top) and without (bottom) an imposed symmetry with respect to the central plane. The top phase diagram is most properly interpreted as phase diagram of a system of half the indicated width, with one neutral wall and one attractive wall. The parallel oriented lamellar phase is denoted by L. The pure cylindrical phase is labeled by C∥, where n represents the number of cylindrical rows lying in the center of the film. The mixed phase with lamellae at the surfaces and cylinders in the center of the film is marked by LC∥, where n represent different numbers of cylinders in the center of the film. For even values of n, the two central cylindrical rows form a rectangular pattern in the top phase diagram, while they form a hexagonal pattern in the bottom phase diagram. The perpendicularly oriented phase is denoted by ⊥. In a two-dimensional system, it is a lamellar phase, and in a three-dimensional system it is a cylindrical phase. The phase diagrams for two- and three-dimensional systems differ only at this place, otherwise they agree with each other (see next section).

Since most of the phase diagram for this system agrees with that of a two-dimensional system, we checked only those regions in parameter space where we expect new structures. We took into account that the possible new morphologies have hexagonal order and selected the periods in the two horizontal directions such that they form the unit cell of a hexagonally packed bravais lattice. (In fact, even when looking at two-dimensional structures, using a three-dimensional system can present an advantage because the minimization of the free energy of a structure with respect to its period parallel to the walls needs to be done only for some discrete values, because the structures can rotate in the cell such that they have their preferred period).

The number of collocation points was at first limited to 64 in each direction by computer memory. We obtained perforated lamellae in parameter regions where in two dimensions the free energy of a lamellar structure is close to that of the equilibrium

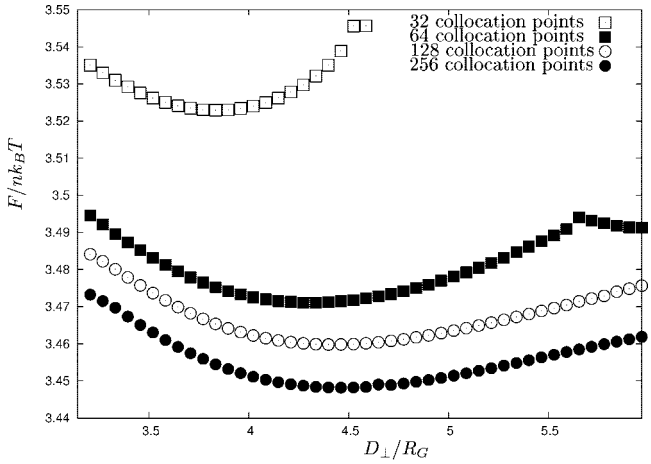

Figure 4. Free energy of the cylindrical phase as a function of the enforced period, for different numbers of collocation points in the two directions. The number of segments of the polymer chain is equal to the number of collocation points. The fixed parameters are $D_{||} = 5.7R_G$ and $\Lambda N = 0.2$.

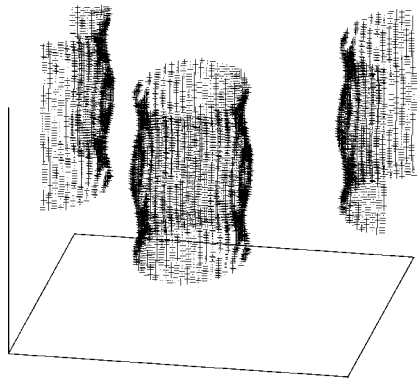

Figure 5. Perpendicularly oriented cylinders in a film of thickness $D_{||} = 2.5R_G$ and $\Lambda N = 0.05$.

morphology, and the perforated lamellar phase was the one with the lowest free energy for some parameter values. However, when we compared the free energies of cylindrical and mixed cylindrical phases with that of the perforated lamellar phase, we found that the free energy of these two morphologies differs only by about 0.5%. Because of the numerical integration and the numerical solution of the differential equations for q and $q^\dagger$ (2) and (3), the inaccuracy in the concentration profiles (and thus in the free energy) is of the same order of magnitude. Even when we only modify the width and height of the step function describing the wall potential (by keeping the area constant), the energies differ by this order of magnitude (see Figure 6). Changing the method of the numerical quadrature also changes the free energies so that another structure may become more favorable. We thus see that different numerical approximations seriously influence the stability of different morphologies. Therefore, it is impossible to decide whether perforated lamellar phases are energetically favorable for the chosen number of collocation points (64^3). Below, we will describe an extended study with far more collocation points, which revealed that perforated lamellae are in fact never the morphology with the lowest free energy, at least for the parameter combinations explored in our simulations.

We also obtained at first undulated lamellae and cylinders with our algorithm, like those reported in ref 18. But these undulated structures are only artifacts of the numerical treatment of the SCFT. They become flat when we impose a more rigorous convergence criterion. While the undulated lamellae and

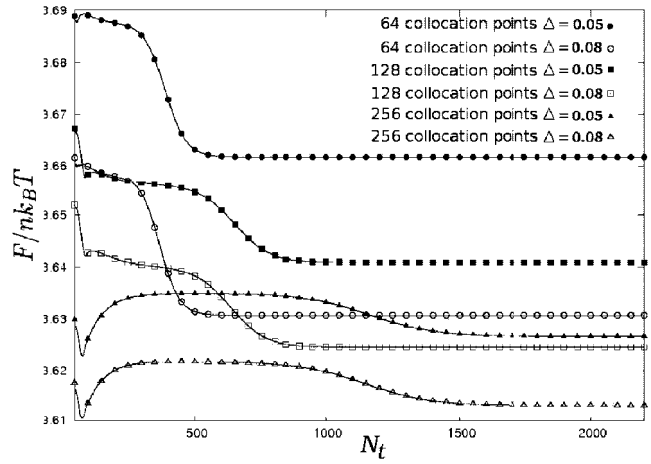

Figure 6. Influence of the implementation of the monomer−wall interaction and of the number of collocation points on the free energy of a pure cylindrical structure. The monomer−wall interaction is implemented as a step function close to the confining walls, with the range and strength of the interaction adjusted such that the area under the step remained constant. The graph shows the free energy as a function of the number of iteration steps N_t. After about 2000 steps the convergence criterion is satisfied. The range of the segment−wall interaction Δ is given in units of $a\sqrt{N}$.

cylinders straighten out, the free energy changes by less than 1%.

For very thin films $\Delta_{||} < 3R_G$, we always found perpendicularly oriented cylinders independently of the affinities. When the walls attract the minority monomer, these cylinders are widened at the walls in order to maximize the favorable contacts (see Figure 5). For thicker films, we found perpendicularly oriented cylinders only for neutral or nearly neutral walls. For walls with a larger affinity for the minority monomer, we did not find perpendicularly oriented cylinders any more because the orientation of the cylinders along the confining walls is energetically favorable. The phase diagram for a three-dimensional system agrees therefore with that of a two-dimensional system; the only difference is that it has perpendicularly oriented cylinders instead of perpendicularly oriented lamellae for very thin films. The phase diagram Figure 3 does not show perpendicularly oriented cylinders for thicker films because the intervall of wall affinities where these are observed is too small.

We conclude this section by an investigation of the perforated lamellae. In order to avoid the above-mentioned problems of numerical inaccuracies, we performed several calculations on a computer with more memory, so that we could compute the morphologies with 128^3 collocation points. We focused on those regions in parameter space where we found perforated lamellae with 64^3 collocation points, since their free energies were very close to those of other morphologies. We found that perforated lamellae do not appear any more when the iteration is performed sufficiently long, even when we start with the perforated lamellae obtained with fewer collocation points. We conclude that the perforated lamellae are only a metastable or weakly unstable structure, which cannot be relaxed into the thermodynamically stable morphology when we take too few collocation points.

Perforated lamellae were found for both positive and negative wall affinities in a number of earlier publications.[14,15,18] In order to compare our work with these studies, we did additional simulations with the volume fraction $f = 0.3$, which is the value chosen in ref 18. Again, more accurate calculations with 128 collocation points and with a finer discretization of the chain disposed of the perforated lamellar phase, for negative and positive wall affinities.

One can understand how perforated lamellae arise by considering the dynamics that occurs in the thin film, starting from a disordered melt. During the dynamics of the SCFT algorithm, the walls' attraction for one of the monomer components first leads to an enrichment of one monomer component at the walls. This results in a depletion of this monomer type in the center, leading to an initial lamellar structure. In order to form nonlamellar morphologies, which have a different symmetry, the polymers have to order in a completely different way. This reordering may require an initial increase in the free energy, in particular when the parameter values are such that the film thickness is close to a multiple of the lamellae's preferred period. Therefore, it is possible that the algorithm remains captured in the lamellar structure, where it can lower the free energy only by perforating the lamellae. This is more likely to happen with fewer collocation points, where the system has fewer degrees of freedom for making rearrangements. Indeed, for negative and positive wall affinities, the perforated lamellae are found in parameter regions where the film thickness is close to a multiple of the lamellae's preferred period.

A similar behavior is observed in two-dimensional systems, where pure lamellar phases are only metastable structures: Here, pure lamellar phases are formed in parameter regions where the film thickness is near a multiple of the lamellae's preferred period. Once the system has formed these lamellae, the algorithm remains captured in this morphology when the number of collocation points is not large enough. It can only get away from the lamellae and form cylinders in the center when we have taken enough collocation points.

We expect that perforated lamellae can only be stable (if at all) in parameter regions very close to the gyroid phase and only if the walls attract the majority monomer. For positive wall affinities, the accumulation of A monomers at the walls leads to even lower volume fractions in the center, where the polymer chains should therefore form cylinders or spheres. Even if the stretching energy is increased slightly compared to the associated bulk phases, because these cylinders or spheres do not have their preferred period, these structures have a significantly smaller surface energy than the perforated lamellae. The cylinders can furthermore decrease their free energy by changing their diameter and thus the period and by changing their shape. Indeed, we typically observed cylinders that are smaller than in the bulk phase and are flattened.

For negative wall affinities, the walls are coated with B monomers, and the volume fraction of A monomers in the center is slightly increased. Only if the system is very close to the gyroid phase, such a shift in the volume fraction can possibly lead to a perforated structure, compared to the cylindrical structures that are otherwise preferred.

These considerations explain our findings that perforated lamellae are not stable in thin films for the volume fractions used in our simulations. The parameter combinations used in the simulations reported in the literature[13,15,18] were even further away from the gyroid phase and therefore we suggest to investigate if perforated lamellae survive in these studies when more collocations points are used. Instead of perforated lamellae, we expect spheres in the center of the film when f is so small that the system is close to the boundary to the spherical phase.

A similar reasoning may be applied to the DDFT study by Huinink et al.[13,14] These authors find perforated lamellae when using polymer chains with nine bonds in a box with at most 32 points in each dimension. When increasing the surface attraction for the minority component in this DDFT study, the morphology changes from cylinders in the center to perforated lamellae, while a wetting layer of A monomers remains at the walls. This is puzzling to us since an increase in surface interaction leads to a further depletion of A monomers in the center, which conflicts with a transition from cylinders to perforated lamellae, which require more A monomers than cylinders do and have larger interfaces. It could be possible that these perforated lamellae occur because the stronger wall affinity imposes an initial lamellar structure, from which the dynamics of the system cannot escape, as outlined above. This hypothesis is supported by the fact that we find perforated and pure lamellae in the same region of parameter space as in this study when we take too few collocation points. However, when we increase the accuracy of our algorithm, we see that these structures are only metastable having a free energy very close to that of the equilibrium morpholgy. These are the reasons why we suppose that perforated lamellae will not stay a stable morphology in DDFT for the investigated parameter values when increasing both the number of points in the box and the chain length. This conclusion is supported by MD simulations[25] for diblock copolymers with volume fractions between 0.35 and 0.45, where it was found that an increase in chain length reduces drastically the region in parameter space where perforated lamellae occur.

Perforated lamellae are also found in ABA triblock copolymer systems. ABA triblock copolymers show a similar behavior to diblock copolymers with the same volume fraction of A blocks. In particular, the theoretical bulk phase diagram obtained by SCFT resembles that of the bulk phase diagram of diblock copolymers.[26] Similarly, the morphologies found in thin films of triblock copolymers are the same as those in thin films of diblock copolymers, and the corresponding phase diagrams resemble each other. Phase diagrams for thin films of ABA block copolymers have been calculated with DDFT[26,28] as well as with Monte Carlo simulations.[29] In the DDFT study perforated lamellae were found in the same region of parameter space as in the study for diblocks.[13,14] Both studies use the same methods, and a triblock copolymer chain used in the new study is identical to two diblock copolymer chains from the first study, when they are connected at the B ends. Apparently, the effect of such a connection on the entropy is so small that the observed phase boundaries change only little. It is beyond the scope of the present paper to judge whether perforated lamellae can be the stable phase for parameter values similar to those used for the diblock copolymer studies, where we have argued that perforated lamellae are only metastable. In Monte Carlo simulations of triblock copolymer melts with χN values considerably higher than those used in our simulations,[29] perforated lamellae were also found. In this study, short chains with a total number of 64 bonds were investigated. For some parameter values the morphologies could not be identified exactly. It appears that the cylindrical bulk structure is not stable within this study because with these chain lengths and temperatures the short A ends align in parallel and are no Gaussian chains. In such a situation, lamellar arrangements are favored. Therefore, this Monte Carlo study is different from the SCFT studies, which are based on Gaussian chains and where cylindrical phases are the bulk morphology.[26]

4. Conclusions

We used a pseudospectral SCFT approach to determine the stable morphologies of an asymmetric AB diblock copolymer confined between two walls that have a preference for one of the monomer types. We investigated a diblock copolymer with volume fraction $f = 0.35$ and a segregation parameter $\chi N = 16$. By varying the film thickness and the affinity of the walls, a phase diagram for a two- and three-dimensional systems was constructed. We considered the case of two identical walls as well as the case of one attractive and one neutral wall. We examined the influence of the numerical accuracy on the stability of possible morphologies. Four types of morphologies were found to be stable for each dimen-

sionality: In two and three dimensions, there occur parallel oriented cylinders, parallel oriented lamellae, and structures consisting of lamellae at the walls and cylinders in the center. Additionally, there occur perpendicular lamellae in two dimensions and perpendicularly oriented cylinders in three dimensions. All morphologies that we found to be stable in three dimensions can be understood as a combination of the cylindrical bulk phase and an increased covering of the walls by the preferred monomer type. The same morphologies were found with DDFT by Huinink et al.[13,14] In addition, they found perforated lamellae for both negative and positive wall affinities. We obtained this morphology also at first, where we used a smaller number of collocation points and of chain segments. The perforated lamellae occurred only in a very small region of our phase diagram, with pure or mixed cylindrical morphologies having a similar free energy. When we took more collocation points, it turned out that perforated lamellar phases are metastable or weakly unstable, and cylindrical phases are the stable morphology in this region of parameter space. We conclude that for the chosen parameter values perforated lamellae are only artifacts of the numerical inaccuracy because they vanish when we increase both the number of collocation points and the number of segments in the chain. We expect that only for a diblock copolymer with f and χN very close to the bulk phase transition between cylinders and lamellae or in the parameter region of the gyroid morphology, perforated lamellae can be the stable phase in a thin film, if at all.

Several authors[14,15,18] report phases with more than one layer of horizontal lamellae. We showed that such phases have a higher free energy than phases that have cylinders in the center.

Other structures, such as undulated lamellae and cylinders, which were found by Yang et al.[18] using real-space SCFT, turned out to be not the morphologies representing the global minimum of the free energy when imposing a stronger convergence criterion or increasing the accuracy of the algorithm.

Our conclusions are based on a careful investigation of the influences of the numerical accuracy on the morphologies and their free energies. We varied the range of the segment−wall interaction and the numerical integration scheme, finding that these details of the numerical implementations can have an influence on the free energy which is for some parameter values of the same order of magnitude as the difference of two adjacent structures. Furthermore, the provided morphologies depend close to the phase boundaries on the initialization of the mean fields. Therefore, it is sometimes impossible to decide which structure is energetically favored. Wherever we encountered this problem, we increased the numerical accuracy of our investigation.

In order to compare our results with results from other work,[14,15,18] we also varied the volume fraction and the segregation parameter. We conclude that a parameter set with a smaller volume fraction and a comparable segregation parameter is not able to stabilize the perforated lamellar phase. We observe for all tested parameters the same behavior, that is, that only the simplest structures remain stable when we increase the number of collocation points and segments in the chain and thus the accuracy of our algorithm. We cannot be sure that a grid of 128^3 collocation points in each dimension is sufficient to correcly capture all features of the phase diagram, but the results obtained with this precision are certainly much better than those obtained on a grid with 64^3 collocation points. Nevertheless, we did a few control simulations with 256^3 collocation points in each dimension. For the three tested parameter combinations, the stable morphology remains the same. Moreover, the morphologies were unchanged when we increased the number of collocation points from 256^2 to 512^2 in a two-dimensional system.

Because of the limitation of the number of collocation points to 64^3 for 2GB memory and 128^3 for 16GB memory, we can only study very thin films with a thickness of a few radii of gyration with sufficient computational precision. We expect that other structures than those obtained in the two-dimensional system will not appear in thicker films because the wall−segment interaction is of short-range, and favorable contacts of monomers with the walls can simply be realized by an enrichment of A monomers at the walls while the bulk structure appears in the center of the film.

It remains to be seen if some of the observed structures depend on the kind of boundary conditions imposed near the walls. While we impose $\phi_A + \phi_B = 1$ everywhere, combined with reflecting boundary conditions at the walls, other authors[18,30] impose a concentration profile that decreases to zero at the walls. Such a change in the boundary conditions cannot produce undulated lamellae and cylinders because such structures are obviously (weakly) unstable. It appears also unlikely to us that such a change in the boundary conditions could stabilize perforated lamellae.

Let us conclude by comparing the results of computer simulations and numerical calculations with those of experiments. Perforated lamellae were observed in experiments with thin films of diblock[30−32] and triblock copolymers,[28] which appear to be very similar to diblock copolymer systems. All these experiments were performed with cylinder-forming block copolymers which were coated on silicon wafers. The films were asymmetric with respect to interactions at the air−film and film−substrate interfaces. In these experiments, various patterns have been reported for diblock copolymers, but no phase diagrams are presented. Since experimental systems differ in many respects from the idealized situation modeled in the theoretical approaches, one cannot conclude with certainty that perforated lamellae cannot be a stable phase in experimental systems in those parameter regoins where they are not stable in theoretical studies. Experimental systems have no Gaussian chains, no reflecting boundary conditions, no rigorous imcompressibility condition, no strict monodispersity, and no fully flat surface. Nevertheless, we suggest that the perforated lamellar phase might be metastable at least in part of the cases where they have been seen in experiments with thin films. There are two reasons for this assumption:

First, the lamellar phase is very similar in free energy to that of cylindrical structures in our theoretical investigations. If this is also true in experiments, the structure that is formed should depend on the initial conditions or on the favored dynamical pathways of the experiment.

Second, in bulk systems the stability of perforated lamellae was discussed for a couple of years until they turned out to be a metastable morphology that is favored during the transition from lamellar to cylindrical phases. Hajduk et al.[34] studied different block copolymer systems and could show that the PL structure is an artifact induced by the sample preparation in each of the studied systems. They pointed out that the perforated lamellar state is a nonequilibrium structure which is converted into the gyroid phase by prolonged isothermal annealing. Vigild et al.[35] approved this result in their study of order−order transitions in different samples of diblock copolymers. Theoretical work by Qi and Wang[36] suggests that the morphology of the metastable perforated lamellae is caused by unstable density fluctuations in the lamellar phase. In thin films this could be the case, too, in particular since perforated lamellae are observed where we expect a dynamical pathway from initially formed lamellae to cylinders. To our knowledge, an investigation comparable to that in refs 34 and 35 in the bulk has not been performed in thin films. Therefore, it is an open question whether and when perforated lamellae are the stable morphology in experimental thin films of diblock copolymers.

Acknowledgment. We thank Marcus Müller for useful discussions and Robert Roth and Christian Fischer for the possibility to perform calculations on their computer cluster. We gratefully acknowledge financial support from the Deutsche Telekom Stiftung.

References and Notes

(1) Leibler, L. *Macromolecules* **1980**, *13*, 1602–1617.
(2) Semenov, A. N. *Sov. Phys. JETP* **1985**, *61*, 733–742.
(3) Matsen, M. W.; Schick, M. *Phys. Rev. Lett.* **1994**, *72*, 2660–2663.
(4) Helfand, E.; Wasserman, Z. R. In *Developments in Block Copolymers*; Goodman, I., Ed.; Applied Science: London, 1982; Vol. 1, pp 99−125.
(5) Bates, F. S.; Fredrickson, G. H. *Annu. Rev. Phys. Chem.* **1990**, *41*, 525–557.
(6) Matsen, M. W.; Bates, F. S. *Macromolecules* **1996**, *29*, 1091–1098.
(7) Khandpur, A. K.; Bates, F. S.; Föster, S.; Hamley, I. W.; Ryan, A. J.; Bras, W. *Macromolecules* **1995**, *28*, 8796–8806.
(8) Lambooy, P.; et al. *Phys. Rev. Lett.* **1994**, *72*, 2899–2902.
(9) Koneripalli, N.; et al. *Macromolecules* **1995**, *28*, 2897–2904.
(10) Matsen, M. W. *J. Chem. Phys.* **1997**, *106*, 7781–7791.
(11) Pickett, G. T.; Balazs, A. C. *Macromolecules* **1997**, *30*, 3097–3103.
(12) Angermann, H. J.; Johner, A.; Semenov, A. N. *Macromolecules* **2006**, *39*, 6210–6220.
(13) Huinink, H. P.; Brokken-Zijp, J. C. M.; van Dijk, M. A.; Sevink, G. J. A. *J. Chem. Phys.* **2000**, *112*, 2452–2462.
(14) Huinink, H. P.; van Dijk, M. A.; Brokken-Zijp, J. C. M.; Sevink, G. J. A. *Macromolecules* **2001**, *34*, 5325–5330.
(15) Wang, Q.; Nealey, P. F.; Pablo, J. J. *Macromolecules* **2001**, *34*, 3458–3470.
(16) Radzilowski, L. H.; Carvalho, B. L.; Thomas, E. L. *J. Polym. Sci., Polym. Phys.* **1996**, *34*, 3081–3093.
(17) Harrison, C.; Park, M.; Chaikin, P. M.; Register, R. A.; Adamson, D. H.; Yao, N. *Macromolecules* **1998**, *31*, 2185–2192.
(18) Yang, Y. Z.; Qiu, F.; Zhang, H. D.; Yang, Y. L. *Polymer* **2006**, *47*, 2205–2216.
(19) Matsen, M. W. *Macromolecules* **2006**, *39*, 5512–5520.
(20) Lin, C.-Y.; Schick, M. *J. Chem. Phys.* **2006**, *125*, 034902.
(21) Honda, T.; Kawakatsu, T. In *Nanostructured Soft Matter*; Zvelindovsky, A. V., Ed.; Springer: Berlin, 2007; p 482.
(22) Matsen, M. W. *Soft Matter* **2006**, *2*, 1048–1056.
(23) Ceniceros, H. D.; Fredrickson, G. H. *Multiscale Model. Simul.* **2004**, *2*, 452–474.
(24) Rasmussen, K. O.; Kalosakas, G. *J. Polym. Sci., Part B: Polym. Phys.* **2002**, *40*, 1777–1783.
(25) Schultz, A. J.; Hall, C. K.; Genzer, J. *J. Chem. Phys.* **2002**, *117*, 10329–10338.
(26) Matsen, M. W.; Thompson, R. B. *J. Chem. Phys.* **1999**, *111*, 7139–7146.
(27) (a) Knoll, A.; Lyakhova, K. S.; Horvat, A.; Krausch; Sevink, G. J. A.; Zvelindovsky, A. V.; Magerle, R. *Nat. Mater.* **2004**, *3*, 886–890. (b) Lyakhova, K. S.; Sevink, G. J. A.; Zvelindovsky, A. V.; Horvat, A.; Magerle, R. *J. Chem. Phys.* **2004**, *120*, 1127–1136. (c) Horvat, A.; Lyakhova, K. S.; Sevink, G. J. A.; Zvelindovsky, A. V.; Magerle, R. *J. Chem. Phys.* **2004**, *120*, 1117–1126.
(28) Knoll, A.; Horvat, A.; Lyakhova, K. S.; Krausch, G.; Sevink, G. J. A.; Zvelindovsky, A. V.; Magerle, R. *Phys. Rev. Lett.* **2002**, *89*, 035501.
(29) Szamel, G.; Müller, M. *J. Chem. Phys.* **2003**, *118*, 905–913.
(30) Geisinger, T.; Müller, M.; Binder, K. *J. Chem. Phys.* **1999**, *111*, 5241–5250.
(31) Tsarkova, L.; Knoll, A.; Krausch, G.; Magerle, R. *Macromolecules* **2006**, *39*, 3608–3615.
(32) Park, I.; Park, S.; Park, H.-W.; Chang, T. *Macromolecules* **2006**, *39*, 315–318.
(33) Lee, B.; Park, I.; Yoon, J.; Park, S.; Kim, J.; Kim, K.-W.; Chang, T.; Ree, M. *Macromolecules* **2005**, *38*, 4311–4323.
(34) Hajduk, D, A.; Takenoushi, H.; Hillmyer, M. A.; Bates, F. S.; Vigild, M. E.; Almdal, K. *Macromolecules* **1997**, *30*, 3788–3795.
(35) Vigild, M. E.; Almdal, K.; Mortensen, K.; Fairclough, J. P. A.; Ryan, A. J. *Macromolecules* **1998**, *31*, 5270–5716.
(36) Qi, S.; Wang, Z.-G. *Macromolecules* **1997**, *30*, 4491–4497.

MA8001627